Title
Cell interaction with three-dimensional sharp-tip nanotopography

Journal
Biomaterials, 28(9)

ISSN
0142-9612

Authors
Choi, Chang-Hwan
Hagvall, S H
Wu, B M
et al.

Publication Date
2007-03-01

Peer reviewed

Cell interaction with three-dimensional sharp-tip nanotopography

[1]Chang-Hwan Choi[1], Sepideh H. Hagvall[2,3], Benjamin M. Wu[2], James C. Y. Dunn[2,3], Ramin E. Beygui[3], and Chang-Jin "CJ" Kim[1]

[1]Mechanical and Aerospace Engineering Department, University of California, Los Angeles, CA 90095, USA

[2]Department of Bioengineering, University of California, Los Angeles, CA 90095, USA

[3]Department of Surgery, University of California, Los Angeles, California 90095, USA

(accepted 22 November 2006)

[1]Corresponding author.
E-mail address: chchoi@ucla.edu (C.-H. Choi).

Abstract

Cells in their native microenvironment interact with three-dimensional (3D) nanofeatures. Despite many reports on the effects of substrate nanotopography on cells, the independent effect of 3D parameters has not been investigated. Recent advances in nanofabrication for precise control of nanostructure pattern, periodicity, shape, and height enabled this systematic study of cell interactions with 3D nanotopographies. Two distinct nanopatterns (posts and grates) with varying three-dimensionalities (50-600 nm in nanostructure height) were created, while maintaining the pattern periodicity (230 nm in pitch) and tip shape (needle- or blade-like sharp tips). Human foreskin fibroblasts exhibited significantly smaller cell size and lower proliferation on needle-like nanoposts, and enhanced elongation with alignment on blade-like nanogrates. These phenomena became more pronounced as the nanotopographical three-dimensionality (structural height) increased. The nanopost and nanograte architectures provided the distinct contact guidance for both filopodia extension and the formation of adhesion molecules complex, which was believed to lead to the unique cell behaviors observed.

Keywords: Nanotopography; Nanopost; Nanograte; Fibroblast; Cell proliferation; Cell morphology; Cell adhesion; Filopodia extension.

1. INTRODUCTION

Cell-matrix adhesion *in vivo* is a three-dimensional (3D) phenomenon that differs from the adhesion on two-dimensional (2D) substrates *in vitro*. The full complement of matrix topography, molecular composition, and mechanical properties (e.g., pliability) are reportedly important for adhesions to form properly and for activation of desired intracellular pathways [1]. Within the extracellular matrix, cells interact with nanoscale topographical projections and depressions that vary in composition, size and periodicity [2]. Topographical features affect cell behaviors in terms of adhesion, morphology, cytoskeletal arrangement, migration, proliferation, surface antigen display, and gene expression [3,4]. The effects of nanoperiodic surface features on the cell behavior had been examined by using nanoscale patterns such as columns [5-12], dots [13-17], pits [18,19], pores [20], gratings [21-26], meshwork [27-30], nanophase grain [31], and random surface roughness [32] created by a variety of nanolithography and nanofabrication techniques including e-beam lithography [23], dip-pen lithography [13], laser irradiation [24], nanoimprinting [12,18,19,26], capillary lithography [10], x-ray lithography [22], interference lithography [21,25], polymer demixing [6,11], block-copolymer lithography [14], nanoparticle or colloidal lithography [7-9,15-17], chemical vapor deposition of carbon nanofibers or nanotubes [27-30], black silicon method [5], electrochemical porous etching [20], chemical etching [32], and thermal sintering [31]. However, the inability to independently control nanodimensionality and nanoperiodicty in the nanoscale range has precluded a systematic study of the 3D effects of nanoscale features on cell behaviors.

The recent achievement in nanofabrication has made it possible to produce well-regulated nanofeatures (nanoposts and nanograte) uniformly over a large sample area (several cm^2) with

independent controllability for feature height (up to 1 μm) and shape (e.g., side-wall profile tip sharpness) [33]. Although interference lithography had previously been used for nanoscale patterning [21,25], its new combination with deep reactive ion etching (DRIE) has enabled us not only to simplify the nanofabrication processes but also to tailor the nanostructures' height and shape three-dimensionally as desired [33]. This report investigates the interactions of human foreskin fibroblasts with the well-defined silicon nanostructures of nanopost and nanograte patterns of varying heights and controlled periodicity. The effects of these nanostructures on cell proliferation, morphology, and adhesion are described.

2. Materials and methods

2.1. Nanostructure fabrication

A simple but effective method to fabricate silicon nanostructures over a large area with superior control of pattern regularity was used, combining interference lithography and DRIE [33], and briefly summarized here. Interference lithography system of Lloyds-mirror configuration using the HeCd laser of the wavelength of 325 nm (Nanotech, University of California, Santa Barbara) was used for the nanopatterning of a photoresist layer spin-coated on a polished silicon substrate (2×2 cm^2). The substrate was then etched by DRIE using the patterned photoresist directly as an etching mask. DRIE etching step determined the nanostructure height and involved the design of etching parameters for sidewall control for positive-tapered profile. Nanostructure with the positively-tapered profile was further sharpened by thermal oxidation and buffered oxide etch (BOE). The sample of 2×2 cm^2 was then cleaved

by using a scriber into four chips of 1×1 cm^2, which was used for multiple experiments guaranteeing the uniformity of the pattern geometries among the chips. Smooth silicon samples (1×1 cm^2) of a polished surface were also prepared as controls. The root mean square surface roughness of the smooth control samples was measured to be less than 1 nm by atomic force microscopy (AFM) over a 10×10 μm^2 scan area.

2.2. Cell culture

Human foreskin fibroblasts (American Type Culture Collection (ATCC, Manassas, VA)) were cultured in Dulbecco´s Modified Eagle Medium (DMEM, Invitrogen, Carlsbad, CA) supplemented with 10% fetal bovine serum (FBS, Invitrogen), penicillin/streptomycin (100 U/ml, Invitrogen). At confluence, cells were detached from the culture dishes by tyrosine/EDTA (Invitrogen) followed by centrifugation (1000 rpm, 5 minutes). The pellet was re-suspended in the culture medium. Before the cell seeding, the samples (nanostructured and control samples of multiple number) were cleaned by the Piranha solution (H_2SO_4:H_2O_2, 3:1 by volume) and the HF (HF:H_2O, 1:50 by volume) dip. Cells were seeded at the density of 1×10^4 cm^{-2} on each sample (1×1 cm^2), which had been placed on polystyrene tissue culture well to contain the culture medium. Cells were kept in culture at 37ºC and 5% CO_2 for 3 days.

2.3. Cell proliferation measurement

The alamarBlue™ assay (Serotec, Raleigh, NC) measures cellular metabolic activity. High levels of metabolic activity indicate cellular viability, and low levels imply cellular toxicity. The

assay utilizes an oxidation-reduction (REDOX) indicator that changes color in response to chemical reduction of the growth medium caused by cell metabolism. After 24 hours, a mixture of alamarBlue™ (in an amount equal to 10% of the total culture volume) and culture medium was aseptically added to the samples. Samples were incubated with alamarBlue™ for 2 hours up to 3 days. The metabolism levels were evaluated on a spectrofluorometer at wavelengths of 570 and 600 nm (the amount of reduced alamarBlue™ is $Absorbance_{570} - Absorbance_{600}$) for each time point.

2.4. Scanning electron microscopy (SEM)

After 3 days of culture, the samples containing human foreskin fibroblasts were rinsed with 0.1M sodium cacodylate buffer, pH 7.2, supplemented with 5% sucrose for 10 minutes and fixed for 30 minutes in 2% Paraformaldehye/2% Glutaraldehyde in 0.1M sodium cacodylate buffer, pH 7.2, supplemented with 5% sucrose, followed by dehydration, 30, 50, 70, 80 and 95% ethanol for 10 minutes each, 100% ethanol for 10 minutes 3 times and finally 100% ethanol for 40 minutes. The samples were dried by incubating in 100% ethanol/hexamethyldisilazane (1:1) for 20 minutes followed by pure hexamethyldisilazane for 20 minutes. Then, the pure hexamethyldisilazane solution was evaporated during 20 minutes air-drying. Once dry, the samples were coated with ~10 nm thick gold/palladium (Au/Pd) by using Denton Desk II sputtering system before examination with a Hitachi S-4700 field emission SEM.

2.5. Image analysis

The SEM images were analyzed by using ImageJ software (free download available at http://rsbweb.nih.gov/ij/) for the quantification of cell density, size, elongation, and alignment. The program used automated detection of cell outline and calculated the number of pixels covered by cells. It also calculated the lengths of the major (longest) and minor (shortest) of a cell by fitting the cell outline to an optimized ellipse shape. Elongation was defined as the length ratio of the major to the minor. Alignment was defined as the angle between the major axis and the zero-angle base line which was set to be parallel to the direction of nanopatterns (see the insets of Figs. 4d and 4e). For the quantification, four images (1 mm^2 each) per sample (four replicates per sample) were taken and averaged. Student's *t*-test (for two samples, assuming unequal variances) was used to compare statistical significance between samples. Results of $p < 0.05$ were considered significant.

2.6. Immunohistochemistry

The samples were fixed in 4% paraformaldehyde for 20 minutes, followed by washing with Dulbecco's phosphate-buffered saline (PBS) for 5 minutes (3 times) and permeabilization by 0.5% Triton X-100 for 10 minutes. Before adding antibodies, non-specific antibody binding sites were blocked by incubating the samples for 30 minutes in blocking buffer (1% bovine serum albumin (BSA), 2% goat serum in PBS). Primary antibody to phosphorylated focal adhesion kinase (Abcam) was diluted in PBS to appropriate dilution, applied on over the samples, and incubated overnight at 4°C, followed by 5 minutes wash with PBS (3 times). Labeled secondary antibody (Alexa Fluor 594, Invitrogen) were diluted in PBS, applied to the samples and incubated for 30 minutes at room temperature. After 5 minutes wash with PBS (3 times),

mounting medium containing DAPI (nuclei staining, Invitrogen) was added to the samples. Digital images were captured of the stained cultures with a digital camera (Optronics, CA) from a Leica DM IRB inverted microscope equipped with 20× (0.40 numerical aperture (NA)), and 100× (1.25 NA) objectives.

3. Results

3.1. Nanopatterned surfaces

The SEM images of the distinct 3D nanotopograhies are shown in Fig. 1. The two different patterns, i.e., 'Nanopost' and 'Nanograte', afforded the investigation of the dependency of cell behaviors on nanopatterns. To further differentiate the 3D effect of the nanotopographies, we varied only the structural height for a given pattern from 'Low' (50-100 nm in height), 'Mid' (200-300 nm), to 'High' (500-600 nm), while keeping the pattern periodicity (230 nm) and the tip shape (needle- or blade-like sharp tip of less than 10 nm in tip apex radius of curvature) fixed. The regular nanoperiodic 3D sharp-tip patterns covered the top surface of each sample with excellent uniformity and regularity (i.e., less than 10% deviation in structural size and shape over a sample [33]).

3.2. Cell number and morphology

Figure 2 shows the viability and proliferation of human foreskin fibroblasts on the 3D nanotopographies, compared to those on the 2D smooth surfaces. Fibroblasts on short 3D

nanostructures ('Nanopost-Low' and 'Nanograte-Low' in Fig. 2) exhibited similar proliferation as those on the control 2D smooth surfaces. However, as the 3D nanotopographical structure became taller or higher ('Nanopost-High' and 'Nanograte-High' in Fig. 2), significantly lower cell viability and proliferation were observed. A more pronounced difference was observed on the Nanopost than on Nanograte samples, suggesting that the cell viability and proliferation were also dependent on the pattern of the nanofeatures, in addition to the nanotopographical three-dimensionality.

While cells on smooth silicon surfaces (Figs. 3a and 3e) exhibited the characteristic morphology on 2D surfaces, i.e., well-spread and flattened, fibroblasts on 3D nanostructured surfaces exhibited significantly different morphology. Although also well-spread and flattened, fibroblasts were slightly elongated on short (50-100 nm high) Nanoposts ('Nanopost-Low' sample, Fig. 3b). On medium (200-300 nm high) Nanoposts ('Nanopost-Mid' sample, Fig. 3c), although elongated as well, the cell size was significantly smaller. On tall (500-600 nm high) Nanoposts ('Nanopost-High' sample, Fig. 3d), fibroblasts exhibited a rounded morphology with a much smaller cell size, indicative of poor adhesion. In contrast, fibroblasts spread well on Nanograte and were more elongated with a clear alignment along the grate direction (Figs. 3f-h). The elongated cell morphology and alignment with the grate direction became more pronounced as the height of Nanograte increased.

The SEM images were used for quantitative image analysis, summarized in Fig. 4. Overall, compared to smooth surfaces, as the 3D nanotopographical height increased, the cell number and the cell size decreased while the cell elongation increased (except for 'Nanopost-High' in Fig. 4c). Smaller cell populations were measured on taller nanostructures, especially on the 'Nanopost-High' sample (Fig. 4a), agreeing with the assessment by alamarBlue™ assay (Fig. 2).

Fibroblasts exhibited enhanced elongation, especially with Nanograte (Fig. 4c), generally preferring to be aligned to the grate patterns they are on (i.e., 0-10° in Fig. 4e). The higher degree of alignment was found on tall Nanograte. Although a noticeable alignment was also measured on Nanopost patterns along the tips or valleys (i.e., 0-10° in Fig. 4d), alignment was most prominent on Nanograte.

3.3. Filopodial interaction

Figure 5 shows that cells use filopodia for spatial sensing in their movement around the nanoenvironment. On the 'Nanopost-Low' (Fig. 5a) and 'Nanograte-Low' samples (Fig. 5d), it was frequently observed that the filopodia extended along the valleys between the nanostructures. Occasionally filopodia were observed to cross over to the next nanostructure (see arrows in Fig. 5d). On the 'Nanopost-Mid' (Fig. 5b) and 'Nanograte-Mid' samples (Fig. 5e), some filopodia extended along the sharp tips rather than in the valleys, as indicated by arrows in the figures. On the 'Nanopost-High' (Fig. 5c) and 'Nanograte-High' samples (Fig. 5f), most filopodia extended along the sharp tips without going into the valleys, as indicated by arrows in the figures. On the 'Nanopost-High' sample (Fig. 5c), the length of the filopodia extension was much shorter than on the other samples.

In cell morphology, the elongated fibroblasts on both Nanoposts and Nanograte aligned along preferred orientations (i.e., 0-10° in Figs. 4d and 4e), with cells on Nanograte aligning more significantly along the engineered nanopattern direction. It should be noted that this direction was identical with the direction where the majority of the filopodia extended, whether it was along the valleys or the sharp tips. The more pronounced alignment of the fibroblasts on the

Nanograte can be explained by the clearer and more directional guidance of the filopodia extension by the anisotropic Nanograte patterns, whereas the less-spread, smaller cell size on the 'Nanopost-High' sample had shorter filopodia extension. This result suggests that the distinct reaction of filopodia to the varying nanotopographies should direct the cell behaviors such as morphology and alignment.

3.4. Cell adhesion

Fibroblasts' adhesions on the 3D nanofeatures were examined by the immunostaining of phosphorylated focal adhesion kinase (pFAK). Fibroblasts on smooth surfaces (Figs. 6a and 6e) and Nanopost surfaces (Figs. 6b-d) exhibited punctuated adhesion complexes, whereas cells on Nanograte surfaces (Figs. 6f-h) demonstrated dash-like adhesion complexes with clear alignment of the adhesion complexes along the direction of the Nanograte pattern. This result is consistent with the enhanced alignment in fibroblasts morphology and filopodia extension on Nanograte surfaces found above, suggesting that 3D nanotopographies also induced distinct intracellular processes that may modify the cell's behaviors.

4. Discussion

To date, there have been several studies on the nanotopographical effects on cell behaviors, including human fibroblasts [6-9,11,15,18,19,23]. Our observations on cell number, morphology, and adhesion on the 3D sharp-tip Nanoposts were consistent with the results reported on the columnar nanostructures fabricated by polymer demixing [6,11] or colloidal lithography [7-9,15],

including a clear interaction between cell's filopodia and the nanofeatures [6,7,9,11]. However, it should be noted that the pattern periodicity (100 nm - 2 μm) and the tip diameter (50 nm - 1 μm) created by the polymer demixing [6,11] were random and varied widely depending on the structure height, making it difficult to directly determine the relative contributions of nanodimension and nanoperiodicity on cell behavior. Similarly, colloidal lithography [7-9,15] still lacked the independent control of the pattern periodicity (60-230 nm depending on the structure height) and tip dimension, not allowing the examination of the importance of symmetry or regularity of the nanotopography [18,34]. Although fewer cells, smaller cell area, clear orientation, more filopodia, and less cytoskeleton activities on regular orthogonal and hexagonal nanopit patterns (100-300 nm in pitch, 35-120 nm in diameter) enabled by e-beam lithography were reported [18,19], the topographical 3D effects were not examinable with the dot or pit patterns. Others have also reported that well-defined micro- and nanoscale grate structures (400-4000 nm in pitch) patterned by e-beam lithography induced fibroblasts' alignment [23]. Although the extensive lateral dimensions covering from nano- to microscale made it possible to explore the effects of lateral arrangements, the ridge width (70-1900 nm) and the groove depth were not regulated, and instead varied depending on the lateral pitches so that the topographical 3D effects of nanoscale grate patterns were not directly explored. By comparison, the combination of interference lithography and DRIE has enabled the simple nanofabrication process to independently tailor the nanostructures' height, shape, and periodicity [33]. In this regard, to the best of the authors' knowledge, our observations are the first systematical results illuminating the unique nanotopographical 3D effects on the cell behaviors, enabled by the well-regulated and uniform sharp-tip nanostructures of varying patterns and heights.

For future studies, the lateral tip size of our sharpened nanostructures (less than 10 nm in tip apex radius of curvature), comparable to that of a single integrin molecule (8-12 nm) in a cell membrane, can provide unique potentials to examine integrin activation and focal adhesion on 3D nanotopographies, which is essential for adhesion-mediated signaling [14]. Our sharp-tip nanotopographies capable of excellent control of nanodimensionality and nanoperiodicity will enable the investigation of the relative contributions and interactions between nanotopographical three-dimensionality and periodicity, on integrin clustering and activation. In addition to the fundamental studies of cell behaviors on nanotopographies, the well-defined nanostructured surfaces have further application possibilities in bioengineering. Fewer cell populations with the retardation of cell growth observed on the sharp-tip tall Nanopost structures suggest that the needle-like nanostructures should be useful for a biological low adhesive surface, i.e., anti-adhesion or anti-fouling surface. The control of bio-adhesion or -fouling only by the surface nanotopographies without any chemical modification will provide many advantages in the designs of lab-on-a-chip microdevices and biomedical implant surfaces. The significant alignment with elongation on the Nanograte topographies also suggests the possibility of changing the cells' orientation or structure by using directional nanostructures, which may be desirable in tissue engineering applications [35]. For instance, nanotopography may be exploited to create cell sheets with specified cell-alignment patterns, and then layers of nanoengineered cell sheets can be stacked to create 3D tissue constructs for tissue regeneration applications.

5. Conclusion

We demonstrated that various nanostructures with controllability of pattern, height, and shape can serve as a new means to elucidate the 3D cell-matrix interactions *in vivo*. The dependency of cell behaviors on nanotopographical three-dimensionality (nanostructural height) was systematically verified for the first time by using well-regulated sharp-tip nanostructures and independently controlling dimensionality and periodicity. As the nanotopographical three-dimensionality increased, the consistent trend of fewer cells and smaller cell size was observed. Compared to 2D smooth surfaces, more elongation was induced on nanostructured surfaces. However, more significant elongation and alignment were presented along Nanograte patterns than Nanoposts, with a higher elongation by taller Nanogrates, illuminating that cell proliferation and morphological characteristics were dependent on not only the type of patterns but also the topographical three-dimensionality. Clear filopodia interactions with the 3D sharp-tip nanotopographies suggested that the nanoscopic filopodial interaction should be closely connected with the microscopic cell morphology such that cells might determine their morphological change, when encountering various nanotopographies, by the filopodia sensing and responsive extension. At the molecular level, the 3D sharp-tip nanotopographies also revealed a marked difference in the formation and arrangement of intracellular adhesion molecules, which would affect the intracellular activities such as gene expression and protein production, in addition to the cell proliferation and morphology. The control of cell adhesion and growth merely by the nanoscale surface topographies can open new application possibilities in bioengineering, especially novel biomaterial design for tissue engineering purpose.

Acknowledgements

This work has been supported by the National Science Foundation Nanoscale Interdisciplinary Research Teams Grant 0103562 and a grant from the Fubon Foundation and American Heart Association.

References

[1] Cukierman E, Pankov R, Stevens DR, Yamada KM. Taking cell-matrix adhesions to the third dimension. Science 2001;294:1708-12.

[2] Abrams GA, Goodman SL, Nealey PF, Franco M, Murphy CJ. Nanoscale topography of the basement membrane underlying the corneal epithelium of the rhesus macaque. Cell Tissue Res 2000;299:39-46.

[3] Flemming RG, Murphy CJ, Abrams GA, Goodman SL, Nealey PF. Effects of synthetic micro- and nano-structured surfaces on cell behavior. Biomaterials 1999;20:573-88.

[4] Curtis A. Tutorial on the biology of nanotopography. IEEE Trans Nanobios 2004;3:293-5.

[5] Turner S, Kam L, Isaacson M, Craighead HG, Shain W, Turner J. Cell attachment on silicon nanostructures. J Vac Sci Technol B 1997;15:2848-54.

[6] Dalby MJ, Pasqui D, Affrossman S. Cell response to nano-islands produced by polymer demixing: a brief review. IEE Proc Nanobiotechnol 2004;151:53-61.

[7] Dalby MJ, Riehle MO, Sutherland DS, Agheli H, Curtis ASG. Fibroblast response to a controlled nanoenvironment produced by colloidal lithography. J Biomed Mater Res 2004;69A:314-22.

[8] Dalby MJ, Berry CC, Riehle MO, Sutherland DS, Agheli H, Curtis ASG. Attempted endocytosis of nano-environment produced by colloidal lithography by human fibroblasts. Exp Cell Res 2004;295:387-94.

[9] Dalby MJ, Riehle MO, Sutherland DS, Agheli H, Curtis ASG. Changes in fibroblast morphology in response to nano-columns produced by colloidal lithography. Biomaterials 2004;25:5415-22.

[10] Kim DH, Kim P, Song I, Cha JM, Lee SH, Kim B, Suh KY. Guided three-dimensional growth of functional cardiomyocytes on polyethylene glycol nanostructures. Langmuir 2006;22:5419-26.

[11] Berry CC, Dalby MJ, McCloy D, Affrossman S. The fibroblast response to tubes exhibiting internal nanotopography. Biomaterials 2005;26:4985-92.

[12] Nomura S, Kojima H, Ohyabu Y, Kuwabara K, Miyauchi A, Uemura T. Cell culture on nanopillar sheet: Study of HeLa cells on nanopillar sheet. Jap J Appl Phys 2005;44:L1184-6.

[13] Lee KB, Park SJ, Mirkin CA, Smith JC, Mrksich M. Protein nanoarrays generated by dip-pen nanolithography. Science 2002;295:1702-5.

[14] Arnold M, Cavalcanti-Adam EA, Glass R, Blummel J, Eck W, Kantlehner M, Kessler H, Spatz JP. Activation of integrin function by nanopatterned adhesive interfaces. ChemPhysChem 2004;5:383-8.

[15] Wood MA, Wilkinson CDW, Curtis ASG. The effects of colloidal nanotopography on initial fibroblast adhesion and morphology. IEEE Trans Nanobios 2006;5:20-31.

[16] Rice JM, Hunt JA, Gallagher JA, Hanarp P, Sutherland DS, Gold J. Quantitative assessment of the response of primary derived human osteoblasts and macrophages to a range of nanotopography surfaces in a single culture model in vitro. Biomaterials 2003;24:4799-818.

[17] Andersson AS, Backhed F, von Euler A, Richter-Dahlfors A, Sutherland D, Kasemo B. Nanoscale features influence epithelial cell morphology and cytokine production. Biomaterials 2003;24:3427-36.

[18] Curtis ASG, Gadegaard N, Dalby MJ, Riehle MO, Wilkinson CDW, Aitchison G. Cells react to nanoscale order and symmetry in their surroundings. IEEE Trans Nanobios 2004;3:61-5.

[19] Dalby MJ, Gadegaard N, Riehle MO, Wilkinson CSW, Curtis ASG. Investigating filopodia sensing using arrays of defined nano-pits down to 35 nm diameter in size. Int J Biochem Cell Biol 2004;36:2005-15.

[20] Sapelkin AV, Bayliss SC, Unal B, Charalambou A. Interaction of B50 rat hippocampal cells with stain-etched porous silicon. Biomaterials 2006;27:842-6.

[21] Clark P, Connolly P, Curtis ASG, Dow JAT, Wilkinson CDW. Cell guidance by ultrafine topography in vitro. J Cell Sci 1991;99:73-7.

[22] Karuri NW, Liliensiek S, Teixeira AI, Abrams G, Campbell S, Nealey PF, Murphy CJ. Biological length scale topography enhances cell-substratum adhesion of human corneal epithelial cells. J Cell Sci 2004;117:3153-64.

[23] Teixeira AI, Nealey PF, Murphy CJ. Responses of human keratocytes to micro- and nanostructured substrates. J Biomed Mater Res 2004;71A:369-76.

[24] Zhu B, Lu Q, Yin J, Hu J, Wang Z. Alignment of osteoblast-like cells and cell-produced collagen matrix induced by nanogrooves. Tissue Eng 2005;11:825-34.

[25] Baac H, Lee JH, Seo JM, Park TH, Chung H, Lee SD, Kim SJ. Submicron-scale topographical control of cell growth using holographic surface relief grating. Mater Sci Eng C 2004;24:209-12.

[26] Yim EKF, Reano RM, Pang SW, Yee AF, Chen CS, Leong KW. Nanopattern-induced changes in morphology and motility of smooth muscle cells. Biomaterials 2005;26:5405-13.

[27] Price RL, Ellison K, Haberstroh KM, Webster TJ. Nanometer surface roughness increases select osteoblast adhesion on carbon nanofiber compacts. J Biomed Mater Res 2004;70A:129-38.

[28] Zanello L, Zhao B, Hu H, Haddon RC. Bone cell proliferation on carbon nanotubes. Nano Lett 2006;6:562-7.

[29] MacDonald RA, Laurenzi BF, Viswanathan G, Ajayan PM, Stegemann JP. Collagen-carbon nanotube composite materials as scaffolds in tissue engineering. J Biomed Mater Res 2005;74A:489-96.

[30] Liopo AV, Stewart MP, Hudson J, Tour JM, Pappas TC. Biocompatibility of native and functionalized single-walled carbon nanotubes for neuronal interface. J Nanosci Nanotechnol 2006;6:1365-74.

[31] Webster TJ, Siegel RW, Bizios R. Osteoblast adhesion on nanophase ceramics. Biomaterials 1999;20:1221-7.

[32] Miller DC, Thapa A, Haberstroh KM, Webster TJ. Endothelial and vascular smooth muscle cell function on poly(lactic-co-glycolic acid) with nano-structured surface features. Biomaterials 2004;25:53-61.

[33] Choi CH, Kim CJ. Fabrication of dense array of tall nanostructures over a large sample area with sidewall profile and tip sharpness control. Nanotechnology 2006;17:5326-33.

[34] Curtis ASG, Casey B, Gallgher JO, Pasqui D, Wood MA, Wilkinson CDW. Substratum nanotopography and the adhesion of biological cells. Are symmetry or regularity of nanotopography important? Biophys Chem 2001;94:275-83.

[35] Desai TA. Micro- and nanoscale structures for tissue engineering constructs. Med Eng Phys 2000;22:595-606.

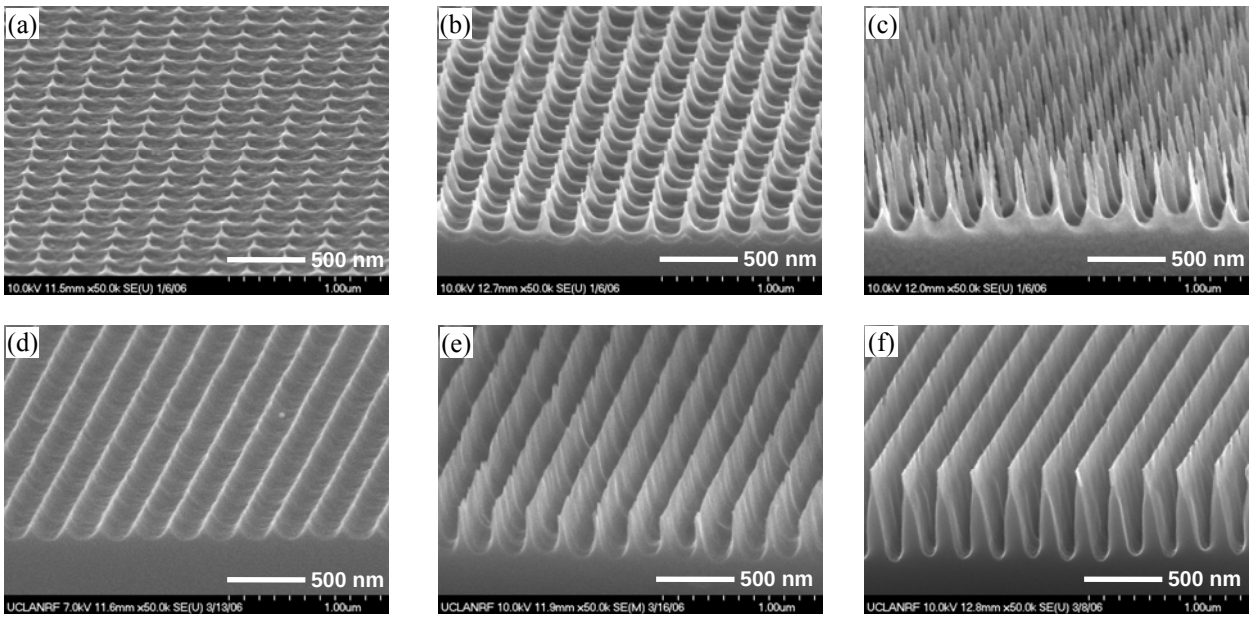

Fig. 1. SEM images of the 3D sharp-tip nanotopography samples of silicon. The well-regulated 'Nanopost' (a-c) and 'Nanograte' (d-f) structures were formed by interference lithography and DRIE uniformly on 2×2 cm^2 silicon substrate, which was then cut into 1×1 cm^2 samples for the study. While the nanostructure pitch was all kept constant to be 230 nm and tips were all sharpened to be needle- or blade-like, structure heights were varied from 'Low' (a, d: 50-100 nm high), 'Mid' (b, e: 200-300 nm high) to 'High' (c, f: 500-600 nm high) to investigate the exclusive effect of the nanotopographical *three-dimensionality* to cell behaviors.

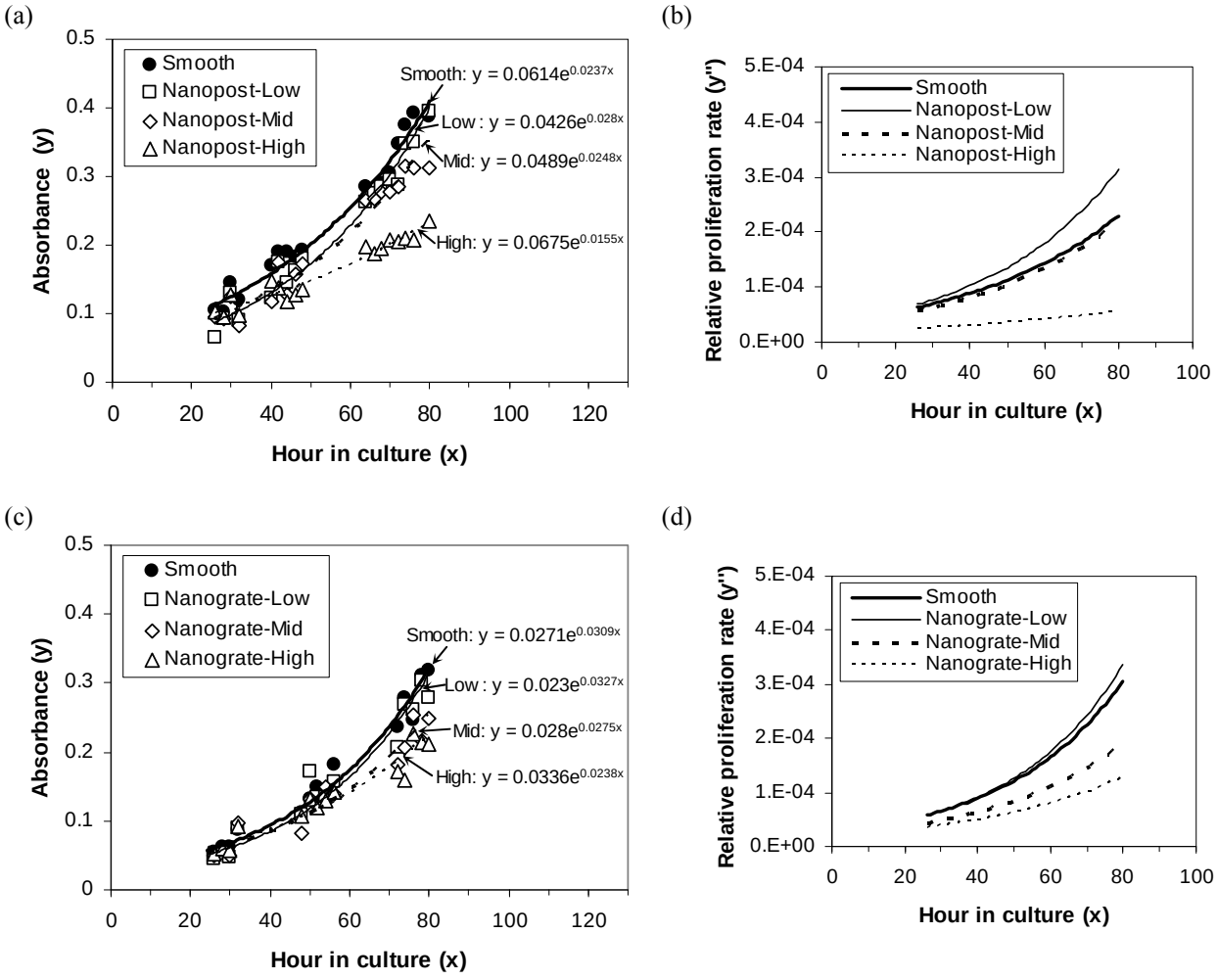

Fig. 2. Cell viability and proliferation on 3D sharp-tip nanotopography. For measurement of fibroblast viability and proliferation over time, the reduction of alamarBlue™ was monitored spectrophotometrically. The measured absorbance value on each sample (a: Nanoposts, c: Nanograte) represents cellular metabolic reduction, which is assumed to follow an exponential trend line. The second derivative of the exponential trend line by time (b: Nanoposts, d: Nanograte) indicates cells' relative proliferation rate. The data for the smooth control sample for Nanoposts and Nanograte were slightly different because the Nanopost group and the Nanograte group each had its own control samples cultured and measured.

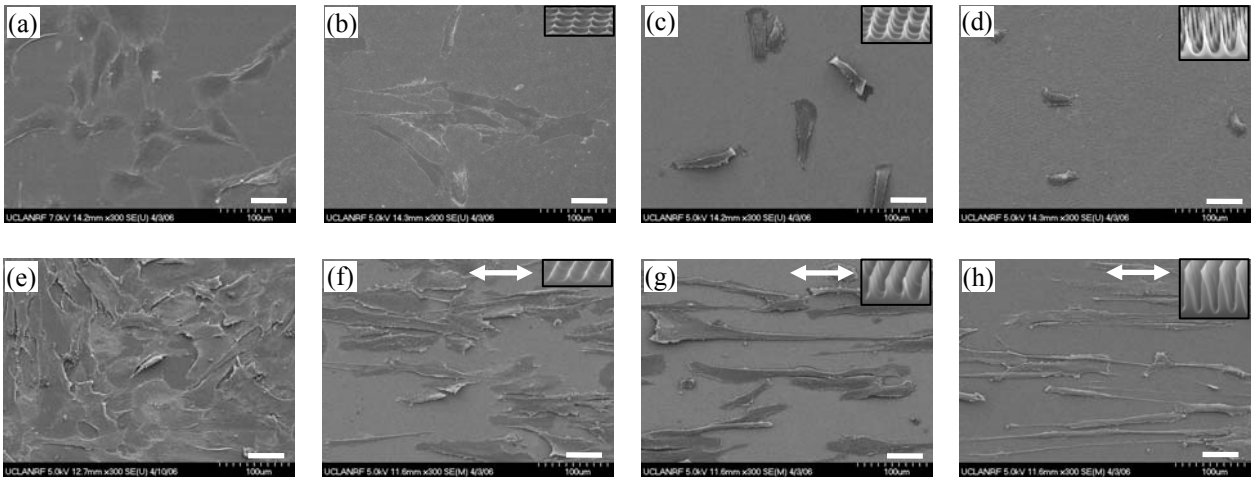

Fig. 3. Cell morphology on 3D sharp-tip nanotopography. To examine fibroblast cells' morphology, the SEM images were taken at the culture periods of 3 days on smooth (a: control for Nanoposts, e: control for Nanogrates), Nanopost (b: Low, c: Mid, d: High), and Nanograte (f: Low, g: Mid, h: High) samples. The scale bar in each image indicates 50 μm. Each inset in (b-d) and (f-h) represents the sample's nanotopography, shown in higher magnification. Each arrow (↔) in (f-h) represents the direction of Nanograte patterns on the sample.

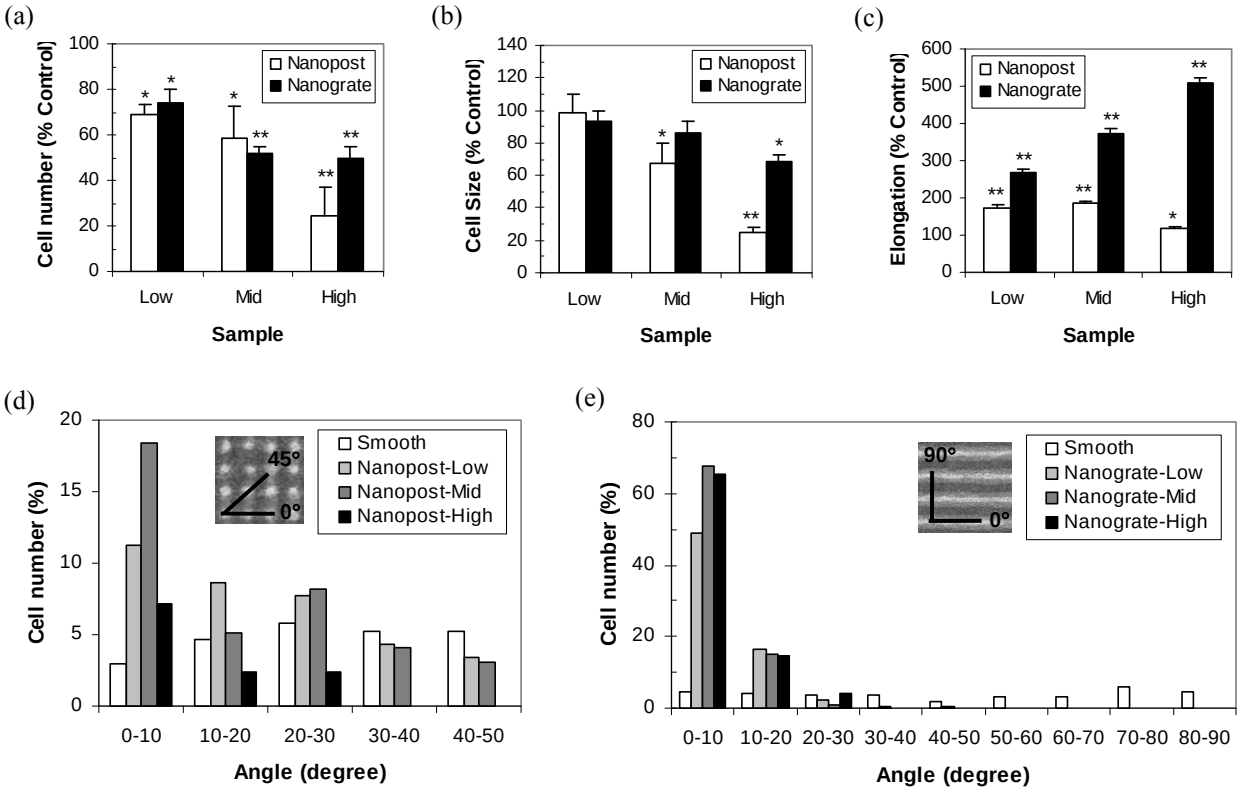

Fig. 4. Image analysis results of cell morphology on 3D sharp-tip nanotopography. By using an image analysis software (ImageJ), the SEM images were quantified to determine cell population (a), size (b), elongation (c), and alignment (d: Nanoposts, e: Nanograte). Figures (a, b, c) indicate the cell numbers, the mean cell sizes, and the mean elongations of cells, respectively, on the nanotopography surfaces, relative to those on the smooth control surfaces. Elongation of cell is defined as the length ratio of the major (longest) to the minor (shortest) of an elliptical cell outline. The results include mean ± standard error of the mean, calculated on means of four images (1×1 mm^2 each) out of multiple samples. Student's *t*-test was performed to evaluate statistical significance between the nanotopography and control samples (* = *t*-test, $p < 0.05$; ** = *t*-test, $p < 0.01$). Figures (d, e) indicate the population of elongated cells in certain orientations relative to the underlying nanopatterns with an interval of 10°. The cells with elongation greater than 3 were counted and expressed as percentage of the total number of cells on the samples. Each inset shows how the angle was defined on each nanopattern. Because of the geometric symmetry, the angles range 0-45° for Nanoposts (d) and 0-90° for Nanograte (e). Because the total number of cells includes those with elongation smaller than 3, the data for each case do not add up to 100%.

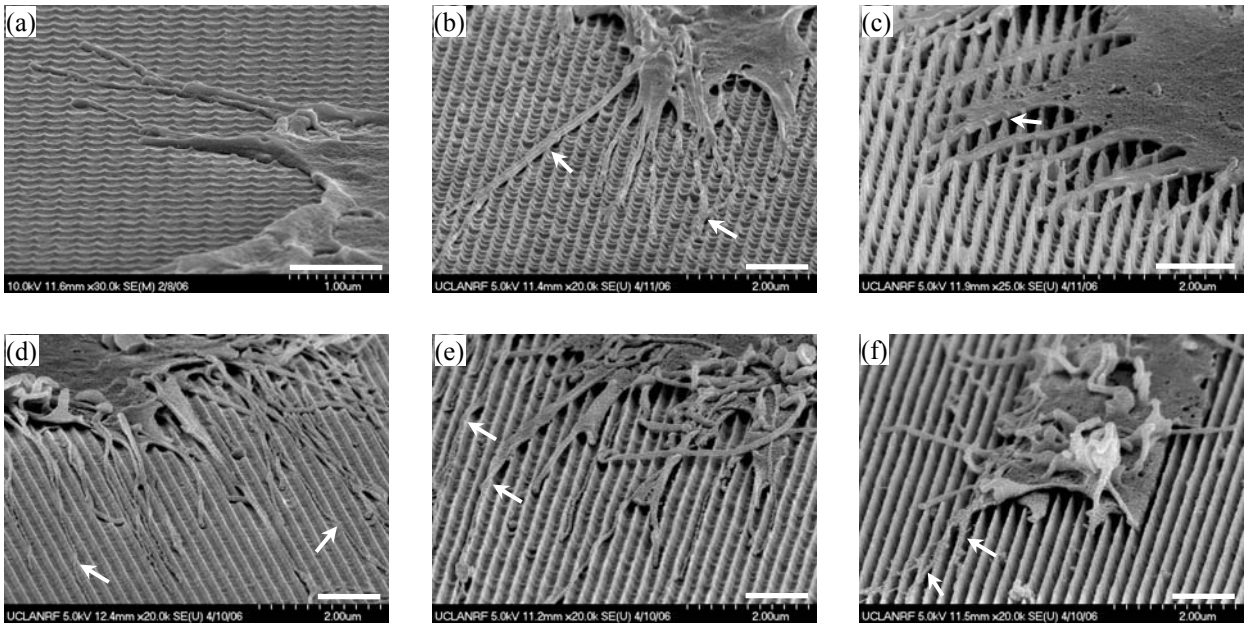

Fig. 5. Filopodial interactions with 3D sharp-tip nanotopography. The SEM images of cells' filopodia were taken at the culture periods of 3 days for Nanopost (a: Low, b: Mid, c: High) and Nanograte (d: Low, e: Mid, f: High) samples. The scale bar in each image indicates 1 μm.

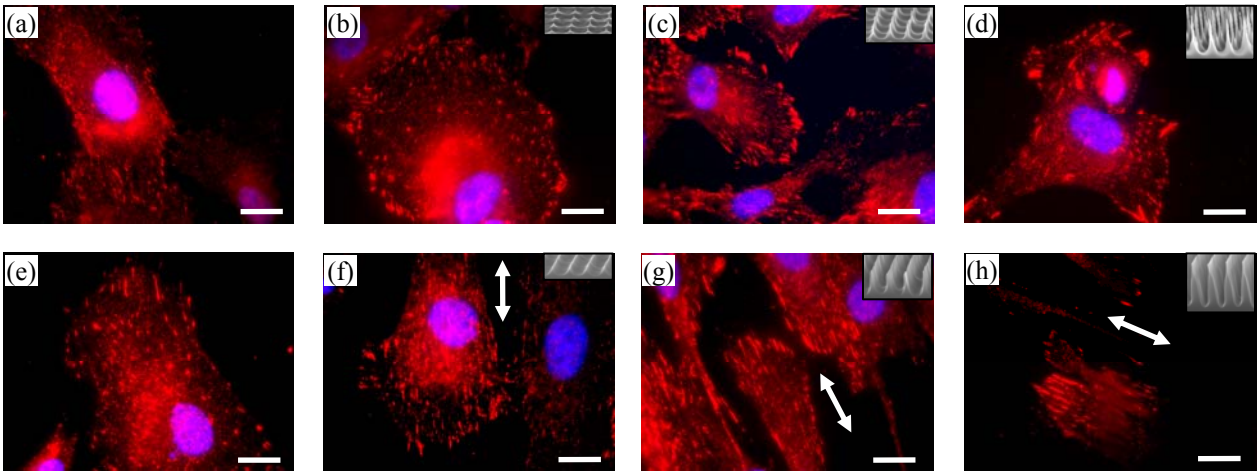

Fig. 6. Cell adhesions on 3D sharp-tip nanotopography. The fluorescence microscope images of immunostaining (nuclei: blue, pFAK: red, in colors) were taken at the culture periods of 3 days for the smooth (a: control for Nanoposts, e: control for Nanogrates), Nanopost (b: Low, c: Mid, d: High), and Nanograte (f: Low, g: Mid, h: High) samples. The scale bar in each image indicates 10 μm. Each inset in (b-d) and (f-h) indicates the nanotopography the cells are on, shown in higher magnification. Each arrow (↔) in (f-h) represents the direction of nanograte patterns on the sample.